Supplemental Data

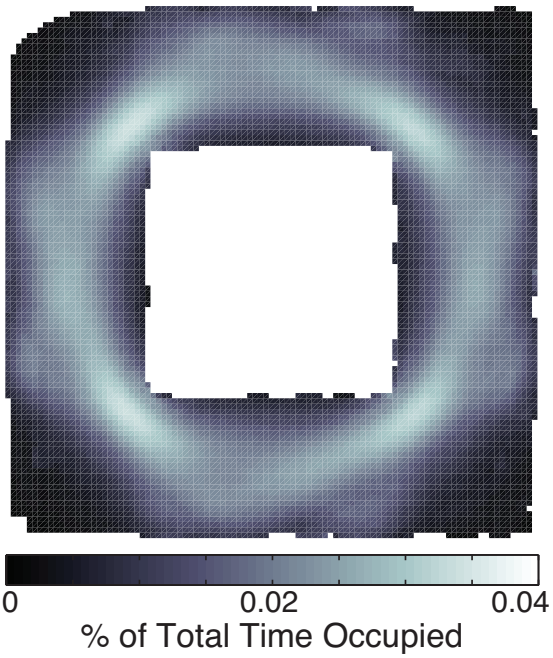

Figure S1: Average occupancy map across all sessions. Brighter shading represents a greater amount of time spent in the region.

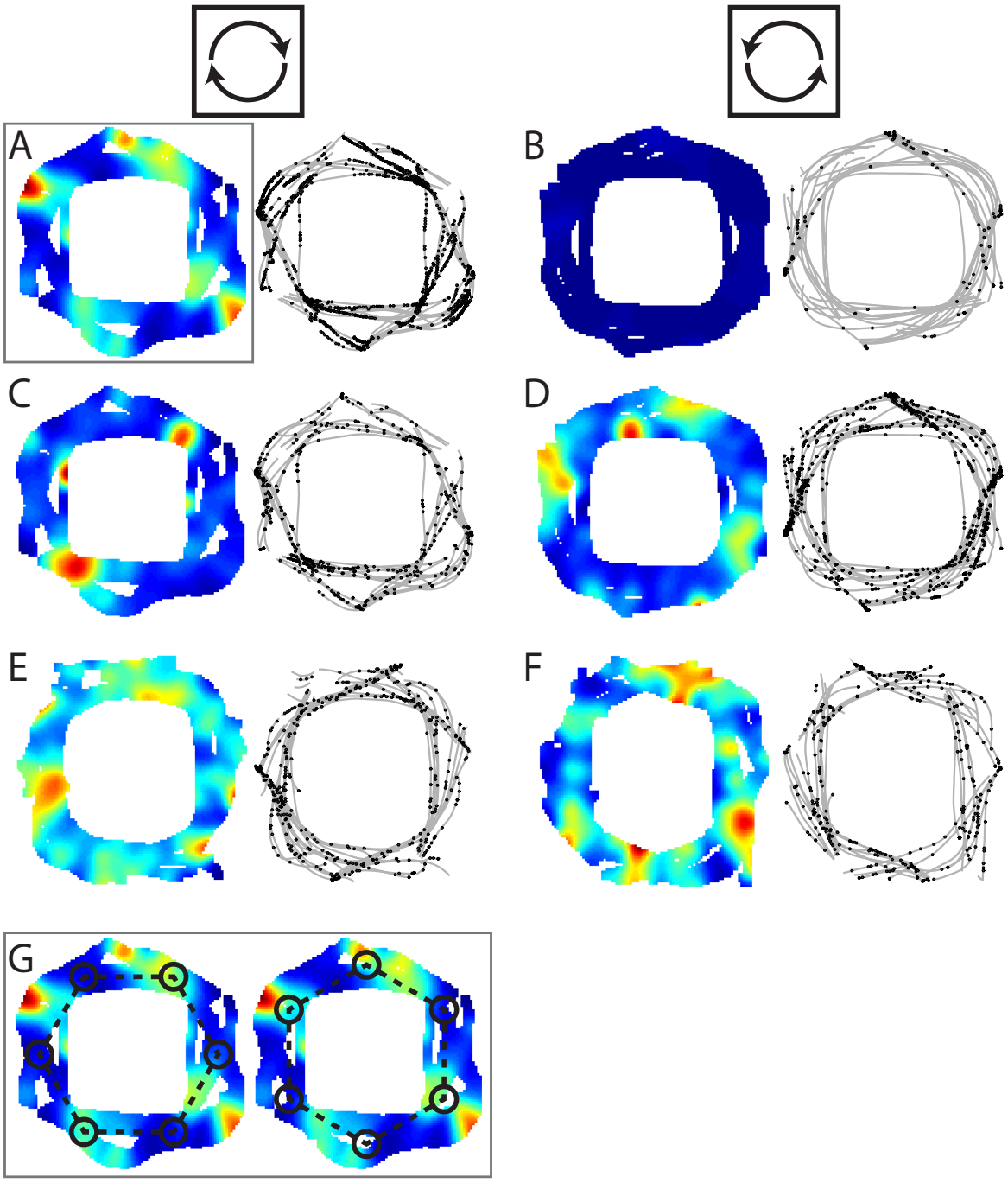

Figure S2: **Firing rate maps and associated spiking activity. A-F.** The rate maps from Figure 2 of the main text are replotted (left) along with the paths taken by the subject and locations where the cell fired, indicated by the gray lines and black dots, respectively (right). *A,C,E:* Clockwise activity for the cells shown in Figure 1. *B,D,F:* Counterclockwise activity for the cells shown in Figure 1. **G.** Firing rate map with an overlaid hexagon for a cell from patient 2's entorhinal cortex (as shown in panel A). The hexagon vertices do not closely fit the locations of the firing peaks, which suggests that our findings are not driven by a conventional grid cell that activates as if in an open arena. *Left:* Unrotated hexagon. *Right:* Hexagon rotated 30 degrees.

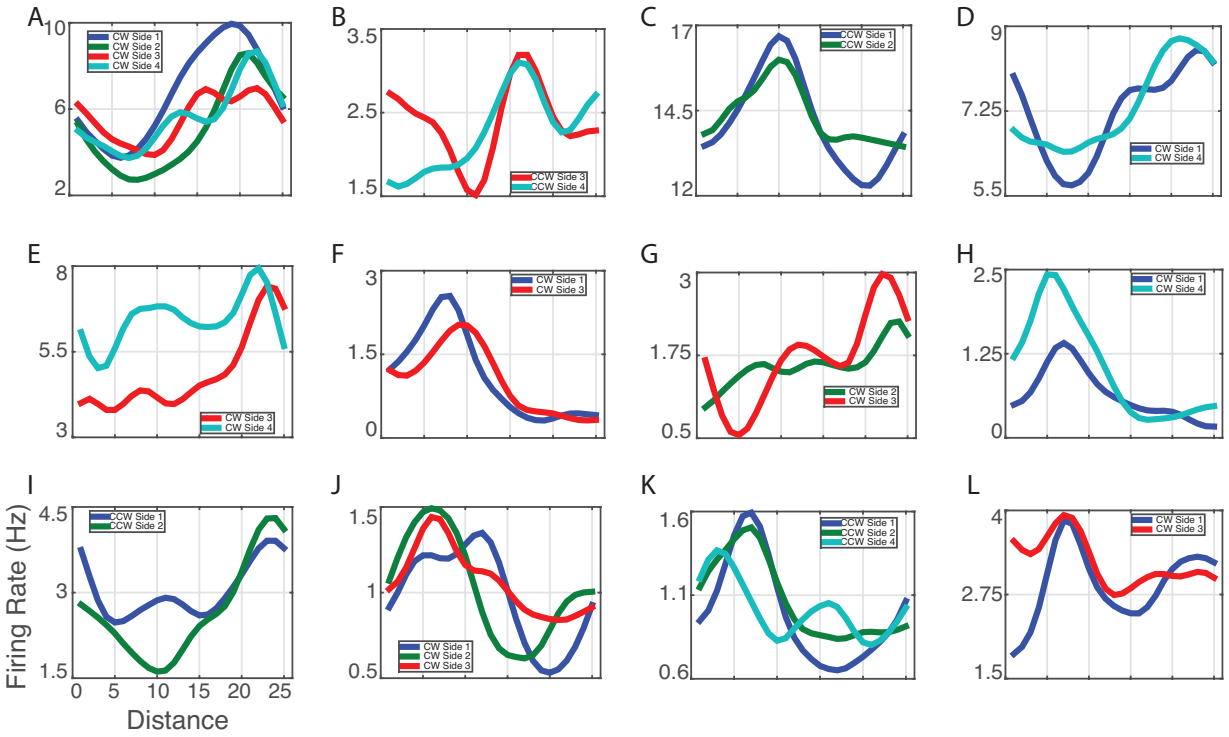

Figure S3: **Additional examples of path equivalent (PE) cells. (A)** A PE cell from patient 2. **(B)** A PE cell from patient 3. **(C)** A PE cell from patient 3. **(D)** A PE cell from patient 4. **(E)** A PE cell from patient 4. **(F)** A PE cell from patient 5. **(G)** A PE cell from patient 6. **(H)** A PE cell from patient 6. **(I)** A PE cell from patient 9. **(J–K)** One PE cell from patient 10 during two different directions of movement. **(L)** A PE cell from patient 11.

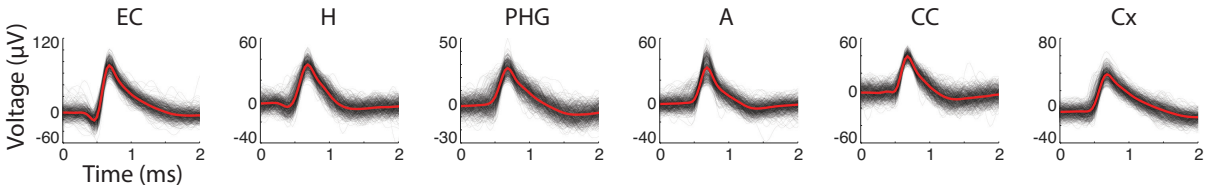

Region	Mean Firing Rate (Hz)	Firing Rate 5%-95% Range (Hz)	Mean Spike Amplitude (μV)	Background noise (μV)	Mean False Positive (FP) Rate	FP below 10%	FP below 20%	Mean False Negative (FN) rate	FN below 10%	FN below 20%
Entorhinal Cortex	4.0	0.1-11.9	44.8	6.8	3.7%	91.1%	95.6%	4.2%	88.6%	94.9%
Hippocampus	2.5	0.1-10.3	42.8	6.7	3.5%	87.0%	96.8%	3.7%	87.7%	95.4%
Parahippocampal Gyrus	2.0	0.1-7.6	36.8	6.1	2.0%	95.7%	97.9%	2.6%	94.7%	95.7%
Amygdala	2.7	0.2-9.7	51.9	6.7	7.6%	77.8%	88.3%	7.5%	77.1%	88.3%
Cingulate Cortex	4.1	0.2-11.8	45.0	8.0	6.7%	79.1%	89.8%	7.4%	76.7%	86.4%
Frontal/Temporal Cortex	3.2	0.2-11.2	42.3	6.9	5.0%	80.3%	92.2%	5.1%	80.3%	91.9%

Figure S4: Spike cluster characteristics. **Top:** Example spike waveforms from each brain region. Red line indicates the mean **Bottom:** Spike cluster isolation metrics. False-positive rate indicates the estimated percentage of spikes that were inappropriately designated as belonging to a given neuron. False-negative rate indicates the percentage of spikes that were caused by a given neuron but were inappropriately labeled as belonging to neighboring neurons or noise. We compared the spike waveforms of path-equivalent cells with those of other neurons and did not find any differences in their mean amplitude (41 μV for path-equivalent cells vs. 45 μV for other cells; $p > 0.35$, ranksum test) or in our false-positive or false-negative rates in distinguishing their waveforms from neighboring cells (p's> 0.1, ranksum tests).

Subject #	EC	H	PHG	A	CC	Cx
1	0 of 0 (0)	0 of 5 (12)	0 of 0 (0)	0 of 3 (20)	1 of 5 (18)	0 of 5 (28)
2	5 of 18 (38)	0 of 6 (27)	0 of 0 (4)	0 of 0 (0)	0 of 9 (40)	0 of 10 (52)
3	0 of 3 (12)	0 of 0 (3)	0 of 0 (0)	0 of 16 (74)	0 of 8 (14)	2 of 10 (47)
4	1 of 6 (32)	1 of 11 (39)	0 of 0 (0)	1 of 5 (39)	2 of 13 (35)	0 of 0 (21)
5	2 of 10 (34)	0 of 7 (45)	0 of 0 (0)	0 of 0 (0)	2 of 7 (38)	0 of 8 (51)
6	1 of 9 (24)	0 of 0 (0)	0 of 0 (0)	1 of 2 (13)	1 of 5 (37)	1 of 10 (32)
7	0 of 0 (0)	0 of 5 (24)	0 of 3 (5)	0 of 7 (23)	0 of 2 (5)	0 of 5 (17)
8	0 of 0 (0)	0 of 6 (39)	0 of 5 (27)	0 of 0 (1)	0 of 0 (0)	0 of 0 (7)
9	0 of 0 (0)	0 of 2 (8)	0 of 0 (0)	0 of 1 (2)	0 of 0 (0)	1 of 3 (9)
10	0 of 0 (0)	1 of 5 (15)	1 of 9 (24)	1 of 9 (28)	0 of 0 (0)	0 of 0 (6)
11	0 of 0 (0)	0 of 6 (26)	0 of 3 (4)	0 of 4 (12)	0 of 2 (19)	1 of 3 (37)
12	1 of 2 (8)	0 of 1 (12)	0 of 3 (22)	0 of 8 (40)	0 of 0 (0)	0 of 0 (0)
13	0 of 3 (10)	3 of 13 (35)	0 of 4 (8)	0 of 3 (14)	0 of 0 (0)	0 of 5 (13)
Total	10 of 51 (158)	5 of 67 (285)	1 of 27 (94)	3 of 58 (266)	6 of 51 (206)	5 of 59 (320)

Table S1: Summary of path equivalent cells by patient and brain region. Counts indicate the number of path equivalent cells out of the total number of location-responsive cells. Numbers in parentheses indicate the total number of cells recorded, regardless of whether a cell was location-responsive. EC: entorhinal cortex; H: hippocampus; PHG: parahippocampal gyrus; A: amygdala; CC: cingulate cortex; Cx: frontal/lateral-temporal cortex.

Supplemental Experimental Procedures

Participants. The task design and methods for data acquisition were described in a previous study that examined this same dataset [S1]. In brief, thirteen patients undergoing surgical treatment for medication-resistant epilepsy participated in the study. All surgeries were performed by I.F. and the research protocol was approved by the University of California, Los Angeles Institutional Review Board. Our dataset is comprised of 35 individual testing sessions (30–50 minutes each), with each participant contributing between one and four sessions. All data analyses and results reported here are novel, although the prior study [S1] did qualitatively describe the activity of one cell we examined here.

Behavioral Task. Patients played a virtual navigation game [S1–S3] on a laptop computer in their hospital room. The virtual environment consisted of six destination stores surrounding the perimeter of a square track, with the center of the environment obstructed by buildings. Patients traveled either clockwise or counterclockwise around the track. Two stores each were located on the east and west walls (sides 2 and 4), and one store each was on the north and south walls (sides 1 and 3). The stores were all visually distinct. The patients navigated the environment using a game controller. On each delivery trial the patient transported a passenger to their requested store destination as accurately as possible. After arrival at the destination, on-screen text displayed the name of the next randomly selected destination store.

Electrophysiology. We recorded spiking activity at 28–32 kHz using 40-μm platinum-iridium microwire electrodes [S4] connected to a Neuralynx recording system. Nine microwires extended from the tip of each clinical depth electrode. The first eight wires were insulated except for their tip and were used to record action potentials. The ninth microwire had its insulation stripped for ~1 cm and served as the voltage reference for the other wires. Action potentials were manually isolated

using spike shape, clustering of wavelet coefficients, and interspike intervals [S5]. We localized the locations of individual electrodes by co-registering post-operative CT scans with pre-implant MRI images and standardizing to a normalized brain [S6]. Assessing entorhinal subregions is an area of ongoing research [S7]. The approach we used to localize within the EC was by performing median splits across extent of our EC electrodes in the lateral/medial, anterior/posterior, and ventral/dorsal axes.

Data Preprocessing. We binned the firing rate of each cell into 100-ms epochs. We labeled each epoch with the patient's location and direction of travel (either clockwise or counterclockwise around the square path). Following previous work on this dataset [S1, S8], epochs without movement and epochs where clockwise or counterclockwise direction was not defined (i.e., when facing towards or away from the center of the environment) were excluded from analysis. With the exception of the firing-rate maps presented in Figure 2A,D,G, all data analyses were conducted after linearizing patients' location along the square path.

Environment Linearization. We linearized the paths of the environment by mapping the angle of every (x,y)-coordinate pair into 1 of 100 sectors, with the width of each sector equal to 3.6°. We used this angular binning scheme because patients' generally followed a circular path during navigation (Figure S1). When viewed in an overhead map, a linearized location value of 1 corresponds to the top-left corner of the environment. Values increase in a clockwise direction around the square path (thus, sectors 1–25 correspond to the top corridor, sectors 25–50 to the right, sectors 51–75 to the bottom, and sectors 76–100 to the left). After linearizing the location, we computed linearized firing rate maps separately for all epochs of clockwise movement and all epochs of counterclockwise movement. Linear firing rate maps were circularly convolved with a 6-sector gaussian window before data analyses.

Location-responsive cells. For each cell, we computed a one-way ANOVA as a screening procedure to identify cells whose firing rate varied significantly according to environment sector [S2]. We separately validated (data not shown) that the outcome of this ANOVA approach is very similar to the information theoretic approaches used by previous studies for this purpose [S9]. We created a distribution of 1000 p-values, each of which was the result of performing the ANOVA on shuffled firing rate maps, whereby the firing rate of the cell was circularly shifted by a random amount relative to the behavioral epochs. In order for a cell to be considered location-responsive, the p-value resulting from the unshuffled data must have been less than 900 of the p-values calculated using the randomly time-shifted data. We performed these calculations separately for epochs of clockwise and epochs of counterclockwise travel. A cell was considered spatially responsive if the true p-value met this criteria for either direction of travel. Note that this screening ANOVA merely identifies cells whose firing rates vary systematically according to location, which is not the same as identifying bona fide place cells, as was performed on this dataset by Jacobs et al. (2010).

Path Equivalent Cells. To determine whether a cell displayed a similar firing patterns across multiple sides of the square track, we used a modified version of the path equivalence coefficient from Frank et al. [S10]. The path equivalence coefficient is a measure of the degree to which a cell fires in similar relative locations on multiple trajectories. Only sides of the track that contained at least one region of three or greater contiguous sectors of elevated firing were included. In this way, our analyses focused on characterizing the specific locations where individual neurons activated, leaving future studies to examine the important issue of why some cells show diminished firing in

areas of certain environments. We define the path-equivalence coefficient as the median correlation between the firing rates of all pairs of included sides minus the median correlation between the firing rates of all pairs of included sides and shuffled sides:

$median(corr(side_i, side_j)) \quad - \quad median(corr(side_i, shuf_j))$

where *side* is the firing rate of the corresponding 25 sectors, $shuf$ is the firing rate of the corresponding 25 sectors shuffled as described below, and i and j range from 1 to the number of included sides. To determine the firing rate values of a shuffled side, we followed the shuffling method of Frank et al. (2000) in which the firing rate values for the first half of the side were reversed and then the values of the two halves were swapped (sequence "A..BC..D" would become "C..DA..B").

To determine whether a cell's path equivalent coefficient value was greater than chance, we created a null distribution of 1000 path equivalent coefficients calculated on permuted data. For each permutation, we circularly shifted the 25 firing rate values of each included side by a random amount, independently for each included side, and recalculated the path equivalent coefficient. If the true coefficient was greater than the 95^{th} percentile of coefficients calculated on shuffled data, then that coefficient was deemed to be significant at $p < 0.05$. This procedure was done twice, one for clockwise movements and one for counterclockwise. If the path equivalent coefficient for either direction of movement was significant, then the cell was classified as a path equivalent cell.

Place field analyses. We also used a shuffling procedure to identify the specific regions of the environment that exhibited significantly elevated firing rates ("place fields") for each cell. For a given cell and circular direction of travel we created a set of 1,000 shuffled firing rate maps, whereby the firing rate of the cell was circularly shifted by a random amount relative to the behavioral epochs. The firing rate within a sector was considered elevated if the activity from the unshuffled data was greater than the 90^{th} percentile of the firing rates for that sector from the shuffled data.

To quantify how often a single cell's place fields appeared at the same relative location on different sides of the path, we computed, for each cell, the degree of relative overlap of each pair of fields. We counted a pair of fields as overlapping if their relative position along each corridor overlapped by at least 50%. To ensure the results were unbiased for each cell, we limited the analysis to only sides with place fields, and divided the number of overlapping pairs by the total number of possible pairs (i.e., pairs of sides with place fields). Counts were combined across clockwise and counterclockwise directions.

In the phenomenon of rate remapping, a cell distinguishes between different spatial representations via variations in the absolute firing rate levels [S11–S14]. We tested whether cells we observed exhibited a related phenomenon in which they varied their firing rates across different fields. For each cell that exhibited two or more fields at the same relative location on different sides of the track (118 cells), we performed an ANOVA comparing the firings rates from when the patient occupied those fields. 8 of these cells (6.8%) significantly varied their firing rates between related fields. This level is not significantly greater than chance (5%) and thus not indicative of rate remapping.

The task's virtual environment exhibits reflective symmetry in that opposite corridors have similar store layouts. There is one store on the east and west corridors and two stores on the north and south corridors (Figure 1A). Given this layout, it was possible that a neural signal related to the quantity or location of nearby stores could masquerade as exhibiting path-equivalence between opposite walls of the environment. We were interested in testing the possibility that path equivalence is related to the presence of nearby landmarks rather than the environment's

overall spatial geometry. For each cell with place fields on exactly two sides, we calculated how often the place fields were positioned on opposite versus neighboring sides. This comparison was important because if two place fields appeared on opposite sides, then they could be driven by the identical store layouts between these areas. In contrast, if place fields were not related to stores, the percent of cells with fields on opposite sides would be at the chance level of 33%. In line with this prediction, 32% of the cells with two place fields had these fields positioned on opposite sides. We separately performed this analysis for cells from each brain region, with no region's percentage significantly differing from chance levels (all p's> 0.1).

Clockwise/Counterclockwise comparison. For each path-equivalent cell, we classified the relationship between the cell's clockwise and counterclockwise firing patterns as either coding relative distance from the start of a corridor, coding absolute location, no relationship, or an ambiguous relationship. We only included cells with at least one place field in both directions of travel, and we only included corridors with a place field. For each included cell, we performed two correlations. First, we correlated mean clockwise activity and mean counterclockwise activity directly such that a significant positive correlation indicates the encoding of location. We then correlated mean clockwise and mean counterclockwise activity with the counterclockwise vector reversed, such that the first position in each vector follows the direction of movement to always represent the corridor's entry point. A significant positive correlation here indicates that a neuron encodes relative distance rather than location. If we observed a significant correlation in both cases (due, for example, to place fields in the middle of the corridors), we classified the relationship as ambiguous.

Supplemental References

[S1] J. Jacobs, M. J. Kahana, A. D. Ekstrom, M. V. Mollison, and I. Fried. A sense of direction in human entorhinal cortex. 107(14):6487–6482, 2010.

[S2] A. D. Ekstrom, M. J. Kahana, J. B. Caplan, T. A. Fields, E. A. Isham, E. L. Newman, and I. Fried. Cellular networks underlying human spatial navigation. *Nature*, 425:184–187, 2003.

[S3] J. Jacobs, C. T. Weidemann, J. F. Miller, A. Solway, J. F. Burke, X. Wei, N. Suthana, M. R. Sperling, A. D. Sharan, I. Fried, and M. J. Kahana. Direct recordings of grid-like neuronal activity in human spatial navigation. *Nature Neuroscience*, 16:1188–1190, 2013.

[S4] I. Fried, C.L. Wilson, N.T. Maidment, J. Jr. Engel, E. Behnke, T.A. Fields, K.A. MacDonald, J.W. Morrow, and L. Ackerson. Cerebral microdialysis combined with single-neuron and electroencephalographic recording in neurosurgical patients. *Journal of Neurosurgery*, 91: 697–705, 1999.

[S5] R. Q. Quiroga, Z. Nadasdy, and Y. Ben-Shaul. Unsupervised spike detection and sorting with wavelets and superparamagnetic clustering. *Neural Computation*, 16:1661–1687, 2004.

[S6] J. Talairach and P. Tournoux. *Co-planar stereotaxic atlas of the human brain*. Verlag, Stuttgart, 1988.

[S7] Usman A Khan, Li Liu, Frank A Provenzano, Diego E Berman, Caterina P Profaci, Richard Sloan, Richard Mayeux, Karen E Duff, and Scott A Small. Molecular drivers and cortical spread of lateral entorhinal cortex dysfunction in preclinical alzheimer's disease. *Nature neuroscience*, 17(2):304–311, 2014.

[S8] J. Jacobs, M. J. Kahana, A. D. Ekstrom, and I. Fried. Brain oscillations control timing of single-neuron activity in humans. *Journal of Neuroscience*, 27(14):3839–3844, 2007.

[S9] Etan J Markus, Carol A Barnes, Bruce L McNaughton, Victoria L Gladden, and William E Skaggs. Spatial information content and reliability of hippocampal ca1 neurons: effects of visual input. *Hippocampus*, 4(4):410–421, 1994.

[S10] L. M. Frank, E. N. Brown, and M. Wilson. Trajectory encoding in the hippocampus and entorhinal cortex. *Neuron*, 27(1):169–178, 2000.

[S11] Gregory J. Quirk, Robert U. Muller, John L. Kubie, and James B. Ranck, Jr. The positional firing properties of medial entorhinal neurons: Description and comparison with hippocampal place cells. 12(5):1945–1963, 1992.

[S12] S. Leutgeb, J.K. Leutgeb, M.B. Moser, and E.I. Moser. Place cells, spatial maps and the population code for memory. *Current Opinion in Neurobiology*, 15:738–746, 2005.

[S13] A.C. Singer, M.P. Karlsson, A.R. Nathe, M.F. Carr, and L.M. Frank. Experience-dependent development of coordinated hippocampal spatial activity representing the similarity of related locations. *Journal of Neuroscience*, 30(35):11586, 2010.

[S14] Kevin Allen, J Nick P Rawlins, David M Bannerman, and Jozsef Csicsvari. Hippocampal place cells can encode multiple trial-dependent features through rate remapping. *The Journal of Neuroscience*, 32(42):14752–14766, 2012.